Progress In Electromagnetics Research M, Vol. 92, 127–136, 2020

Vector Magnetic Near-Field Measurement in Unit Cell of Metamaterial

Yingyi Qi[1], Zehua Gao[1, #], Chuwen Lan[1], Maopeng Wu[2], and Qian Zhao[2, *, #]

Abstract—Near-field magnetic measurement is a simple but effective way of researching the magical electromagnetic properties of metamaterials. However, till now, the experiments in the field of metamaterials have involved only far-field macroscopic and near-field electric measurements because of the difficulty in isolating interference from electric fields. In this research, we design and fabricate a near-field magnetic probe with about an one-tenth wavelength size and 20 dB E-field rejection ratio, which can be combined with a parallel double-plate device integrating a system for measuring anisotropic vector magnetic field. As a verification measurement of plane waves and cylindrical waves, it got the clear vector field distribution characteristics and good anisotropy. Next we used the dipole to measure the typical metal split ring structure of the metamaterial. The measurement of the distribution of magnetic fields contributes to revealing the interaction mechanism between electromagnetic waves and metamaterials as well as the relationship between microscopic structural elements and macroscopic electromagnetic properties.

1. INTRODUCTION

Metamaterials are artificial electromagnetic media based on man-made atoms, with distinct properties not observed in natural materials [1]. Specific electromagnetic parameters or functions rely mainly on different unit cells. The main methods to study the properties of metamaterials are to gain the equivalent permittivity ε and magnetic permeability μ by measuring transmittance S_{21}, reflectivity S_{11}, and other scattering characteristics related to the effective medium theory [2]. To some extent, although effective electromagnetic parameters can be used to characterize the macroscopic electromagnetic properties of materials, the microscopic electromagnetic response is the fundamental cause of macroscopic electromagnetic properties. Given the size effect of the sub-wavelength, the electromagnetic response of a microstructure is essential to clarify the design, implementation mechanism, and performance optimization of the metamaterial. It is relatively convenient to run the electric field test by using a simple electric dipole probe. At present, near-field characteristics are mostly reflected in an electric field.

Over the past several years, the electric field measurement of metamaterial has made remarkable progress. Under this measurement method, many special phenomena and functionalities have been verified by the intuitive electric field distribution, including negative refraction effect [3, 4], invisibility cloak [5–8], omnidirectional electromagnetic absorber [9], zero-Phase delay [10], negative permeability [11], two-dimensional diffuse reflection [12], etc. Nevertheless, some special metamaterial structures, such as toroidal dipole modes [13–16], need local magnetic field distribution observation, and there are many corresponding theoretical and simulation studies. As the lack of electromagnetic field

Received 14 January 2020, Accepted 26 April 2020, Scheduled 11 May 2020
* Corresponding author: Qian Zhao (zhaoqian@tsinghua.edu.cn).
# Zehua Gao and Qian Zhao have made the same contribution to this paper.
[1] Beijing Laboratory of Advanced Information Networks & Beijing Key Laboratory of Network System Architecture and Convergence, School of Information and Communication Engineering, Beijing University of Posts and Telecommunications, Beijing 100876, China.
[2] State Key Laboratory of Tribology, Department of Mechanical Engineering, Tsinghua University, Beijing 100084, China.

distribution measurement more intuitively reflects on toroidal dipole modes, the experimental part of most articles only involves the transmission S_{21}. Xu et al. first observed the electric field distribution results of the toroidal dipole modes based on the trimmer all-dielectric metasurface in 2018 [16], which is of significance for the development of the toroidal dipole mode. However, circular magnetic field distribution is representative for magnetic toroidal dipole modes [13]. In such a case, magnetic field traits are more intuitive than electric field, serving as a critical means for characterizing and studying toroidal dipole modes.

However, the coupling of magnetic field measurement and electric field brings challenges in the high-frequency magnetic field test in microwave band, that is, the higher the frequency band is, the stronger the influence of the electric field component is. Plus, the bare loop antenna in the X-band could not be effectively measured. Meanwhile, owing to the high-frequency band, the size of the loop is required to be smaller. Moreover, the symmetry of the torus has a great influence on measurement precision, which brings higher requirements on the processing technology. It is of great meaning to research and develop a corresponding magnetic field test dipole to achieve high spatial resolution and high sensitivity test.

In order to tackle the above problems, we designed and prepared a magnetic field measuring dipole to acquire high spatial resolution, anisotropic measurement, and sensitivity of magnetic field response. The dipole was utilized to test the magnetic field near the metal split ring so as to obtain accurate magnetic field distribution results. This method can effectively reveal the microscopic working mechanism in the unit cell of metamaterials.

2. THEORETICAL ANALYSIS

To further explain the reception of electromagnetic wave, we analyzed a shielded loop antenna as shown in Fig. 1(a). The structure of the shielded loop antenna is divided into three parts: the outside of the shielded layer is the receiving antenna; the inside of the shield layer and the inner conductor form a transformer; and the gap is the feed point. The incident electromagnetic wave will induce a voltage on the gap of the shield which in turn stimulates the current on the inner wall of the shield. Then, the current flowing through the shield is coupled to the inner conductor via the inductive field and passes through the coaxial line structure (the inside of the shield layer and inner conductor form a coaxial line structure) coupled to the receiving end, which can constitute an ideal natural balun structure for any frequency. It is important to note that the gap structure is indispensable. Otherwise, due to the skin effect, the signal can only induce a current outside the shielding layer and cannot enter the receiving end.

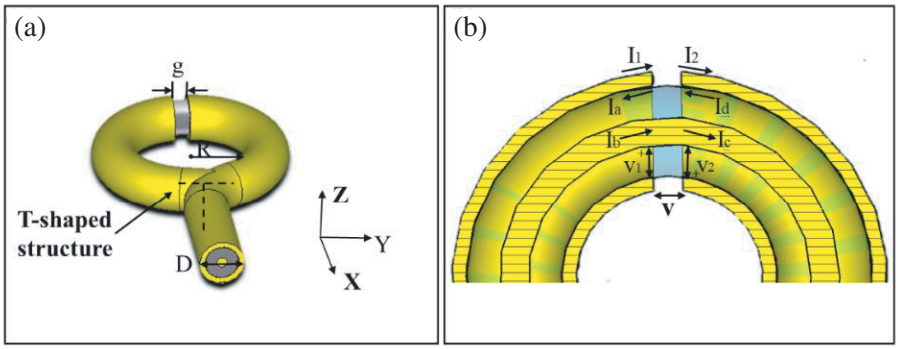

Figure 1. Analysis of structure and principle of shielded loop antenna. (a) Shielded loop antenna model (coaxial transmission line feed). (b) The current and voltage distribution at the gap of the shield loop antenna.

Incident electromagnetic waves will induce a voltage in a conductor formed by the outer surface of the shield. When the shielded layer is continuous, the induced current is limited to the outer surface of the shielded layer (except the gap) through the skin effect, and the current and voltage distributions at

the gap are analyzed (Fig. 1(b)). The shielded layer can be divided into left and right sections from the gap, and the current of the shielded loop can be simply analyzed by Kirchhoff's law and transmission line theory. The currents I_1, I_2, I_a, I_b, I_c, and I_d are equal in magnitude.

Analyze the impedance at the gap. The input impedance $Z_1 = V_1/I_a$ in the left half is determined by the impedance between the outside of the inner conductor and the inside of the left half shield. The inner conductor and outer shield are shorted at the bottom of the loop. Z_1 is equivalent to a very small inductance. The input impedance of the right half is $Z_2 = V_2/I_d$. The external load is a transmission line, so $Z_2 = Z_0$. The load impedance presented at the gap is $Z = V/I_1$, which is $(V_1 + V_2)/I_1$ or $Z_1 + Z_2$.

Due to the symmetry of the antenna and the coaxial transmission line, the components of the uniformly distributed induced current flowing on the outer conductor of the shield reach the same components at the midpoint of the T-shaped structure and can cancel each other. There is no current outside the shield of the vertical portion of the transmission line, and no vertical polarization interference is introduced (for all frequency). In addition, the input impedance seen from the gap is Z_1+Z_2, which is close to the characteristic impedance of the transmission line, perfectly solving the impedance matching problem.

Secondly, it is theoretically proved that the size of the measuring pole that we designed is reasonable for the applied frequency. The near-magnetic field can be effectively measured without the influence of the electric field component. To further explain the reception of electric and magnetic fields, we analyze the bare-loop antenna as shown in Fig. 2(a), where Z_L represents the impedance of the measuring device, and a and b are the conductor radius, and loop radius ($b \gg a$).

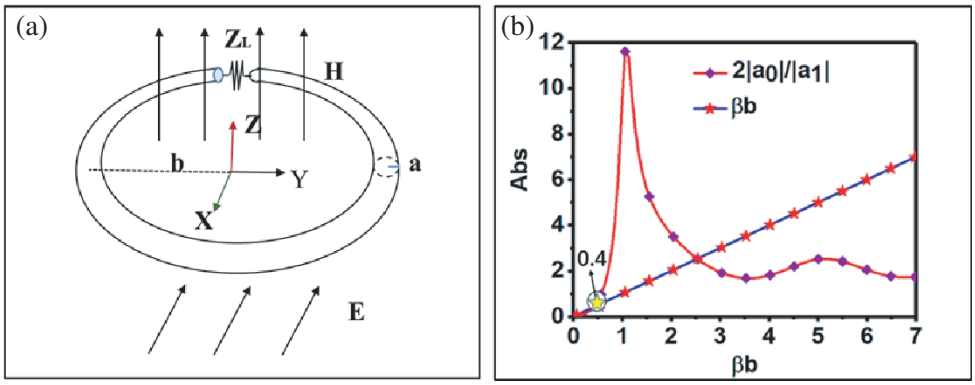

Figure 2. Analysis of structure and principle of loop antenna. (a) Schematic diagram of loop antenna. (b) The magnitudes of $|a_0|/|a_1|$ and βb are shown in the figure, which are the numerator and denominator of Eq. (6).

At lower frequencies [17], $\frac{1}{\omega C} \gg \omega L$ (L, C are the self-inductance and self-capacitance of the small loop, respectively), and the radiation resistance in series with L and C is negligible, using the equivalent circuit analysis, the ratio of the magnetic field response to the electric field response is

$$\left|\frac{V_{oh}}{V_{oe}}\right| \propto \frac{c}{4\pi bf} \tag{1}$$

where c is the speed of light in free space, and f is the measuring frequency. As can be seen from the above equation, when the frequency f rises, the ratio of the magnetic field to the electric field response drops, and the interference of the electric field increases, which make the measurement of the high-frequency magnetic field more difficult.

From the viewpoint of antenna theory [18] and basic theory of the electromagnetic field, the error of measuring the magnetic field of the electric small loop antenna is put into study. When the magnetic field is perpendicular to the torus (both the electric field and the incident wave are in the torus), the actual measured port voltage is

$$V\left(Z_L{=}\infty\right) = E_0 h_e\left(\theta, \phi_i, \psi\right) \tag{2}$$

where E_0 is the intensity of the incident electric field, h_e the effective electrical length, and ϕ_i, ψ, θ represent the angles between each point on the spherical coordinate system and the x-axis, y-axis, and z-axis, respectively. The key Eq. (3) is further derived from Eq. (2).

$$V\delta(\phi) = \frac{j\zeta_0}{4\pi}\int_{-\pi}^{\pi} M(\phi-\phi')I(\phi')d\phi' \tag{3}$$

Here $\delta(\phi)$ is the impulse function; $\zeta_0 = \sqrt{\mu_0/\varepsilon_0}$; ε_0 and μ_0 are the vacuum permittivity and permeability; $M(\phi-\phi')$ is the convolution kernel function; $I(\phi')$ is the distributed current on the loop. Through a series of equation derivation, the result can be obtained accordingly.

$$\beta h_e\left(\frac{\pi}{2}, 0, \phi_i\right) = \frac{1}{1+2a_0a_1^{-1}}\left(j\pi b^2\beta^2 + \frac{2\pi b\beta a_0}{a_1}cos\phi_i\right) \tag{4}$$

where a_0 and a_1 are coefficients of the Fourier series expansion of $M(\phi-\phi')$; $\beta = 2\pi/\lambda$; β and λ are the wave number and wavelength of the incident wave, respectively.

The first and second terms on the right-hand side of Eq. (4) are the contributions of the magnetic field and electric field to the port voltage, respectively, and the ratio of V_E/V_H is calculated.

$$\frac{V_E}{V_H} = \frac{\frac{2\pi b\beta}{a_1}\cos\phi_i}{j\pi b^2\beta^2} \tag{5}$$

Take $\phi_i = \pi$ (that is, the electric field is perpendicular to the port gap direction of the ring, and an induced voltage can be generated at the gap). With the worst case considered, the electric field has the largest interference, and the modulus of the equation above can be converted into

$$\left|\frac{V_E}{V_H}\right| = \frac{2a_0/a_1}{\beta b} \tag{6}$$

When $\beta b \ll 1$ (meeting the requirements of the electrical small loop) and $2a_0 \ll \beta b a_1$ are satisfied, the electric small loop antenna can be effective on measuring the vector magnetic field, and the reception effect is analyzed by taking 10 GHz as an example.

According to Fig. 2(b), it is of necessity to satisfy the voltage generated by the magnetic field to occupy the dominant position. While satisfying the requirement of the electric small loop $\beta b \ll 1$, it is also essential to satisfy $\beta b \ll 0.4$, and the required radius is much smaller than 2 mm. We have chosen an appropriate measuring pole size (<4 mm) to ensure that the magnetic field component acts dominantly.

The shielded loop antenna is utilized to measure the two perpendicular magnetic fields in a two-dimensional plane, and the field distribution in two directions is synthesized by a vector synthesis method. A classical metal split ring structure can be measured by using a shielded loop antenna, which is also used as a prototype for many metamaterial units in the research. Observing the regulation of the magnetic field can help us understand the mechanism of metamaterial in essence.

3. EXPERIMENTAL

3.1. Experimental Measurement Equipment and Shielded Loop Antenna Production

The field scanning device that we used is shown in Fig. 3(a). Microwaves are introduced into the chamber through an X-band waveguide adapter or coaxial antenna to stimulate plane or cylindrical waves. The probe is mounted in the center of the upper plate, and the source and sample are fixed to the lower plate. The lower backplane is connected to a computer-controlled orthogonal XY linear platform for automatic scanning. A shielded loop antenna served as a probe is coupled with the device to scan and measure a two-dimensional magnetic field distribution, observing the magnetic field distribution feature.

The coaxial shielded loop antenna is processed to measure the high-frequency magnetic field. The dimensions of the proposed antenna are finally optimized as follows: $R = 4$ mm. $D = 0.86$ mm, $g = 0.2$ mm. In addition, the gap position needs to be in the center position of the whole structure, ever since the symmetry of the gap position influences the measurement result. The coaxial line is so thin that the damage rate goes up. In the meantime, the manufacturing process is dragging and laborious to make sure of the symmetry of the torus.

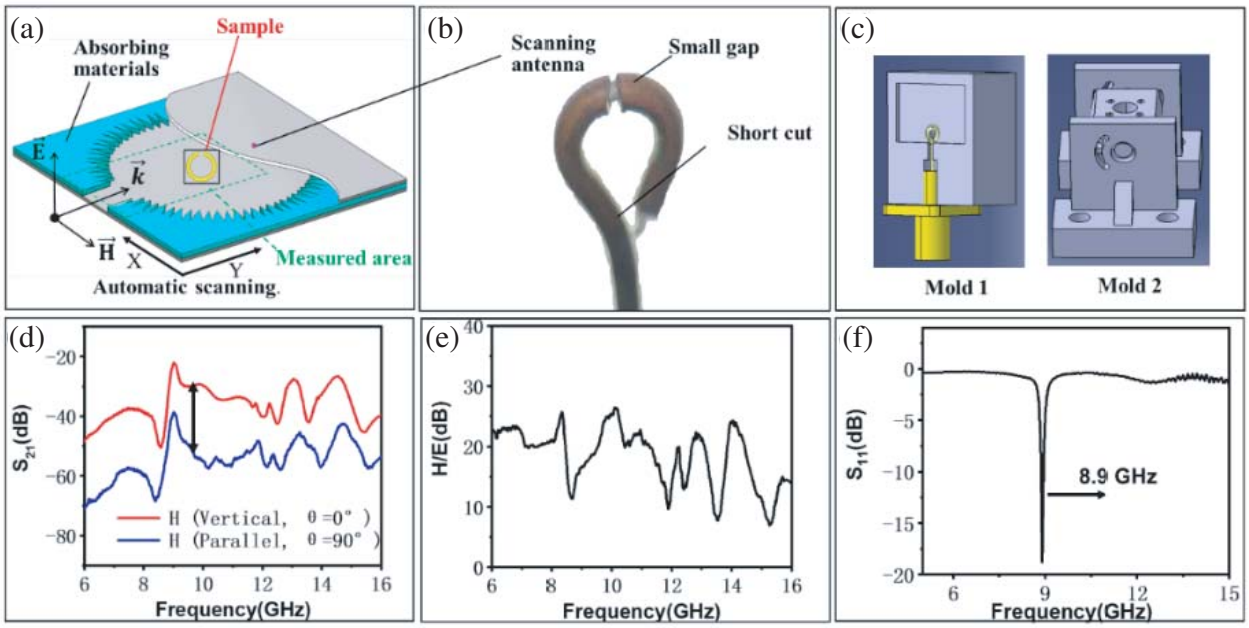

Figure 3. Experimental measurement of the fabricated near-field magnetic probe. (a) Magnetic-field measurement system. (b) Microscope image of a laser cut sample. (c) Schematic diagram of mold. (d) Measured S_{21} response in the case where the near-field magnetic probe is perpendicular and parallel to the magnetic field. (e) Electric field suppression ratio measured by the probe. (f) S_{11} parameters of the antenna.

In order to ensure the symmetry of the shielded loop structure and improve the success odds, we consider using molds combined with laser processing technology for stable batch processing. The 3D-printed mold structure is shown in Fig. 3(c), which mainly includes two sets of molds to perfectly design the size of the small ring, control the symmetry of the torus processing, and coordinate the positioning of the subsequent laser processing. Then next, the performance of the shielded loop structure etched by laser is evaluated by experimental measurement.

3.2. Probe Characteristics

Before the measurement, the standard parts of the vector network serve as calibration, and the interference inside the vector network and the interference of the coaxial cable are removed, and the plane wave field source is measured in the parallel plate device. Fig. 3(d) shows the experimentally-measured response S_{21} when the loop is perpendicular and parallel to the magnetic field. Fig. 3(e) tells the electric field suppression ratio (or electric field isolation, defined as the ratio of the received magnetic field component and electric field component in the received signal) measured by the probe, that is, the ratio of the amplitude of a signal received when the loop is perpendicular to the magnetic field or parallel to the magnetic field. It has good anisotropy in a wide frequency range from 6 GHz to 16 GHz (including the resonance frequency). The isolation of the electric and magnetic fields is around 20 dB around 10 GHz.

The S_{11} parameter of the antenna serves as a reference value for the effective measurement frequency range of the antenna. As shown in Fig. 3(f), the resonant frequency is about 8.9 GHz.

3.3. Empty Field Measurement

Two types of source fields were measured without any sample to evaluate the performance of the measuring device: a plane wave and cylindrical wave. Comparing the measurement results of the designed coaxial shielded loop antenna and the bare loop antenna (the size parameters are the same,

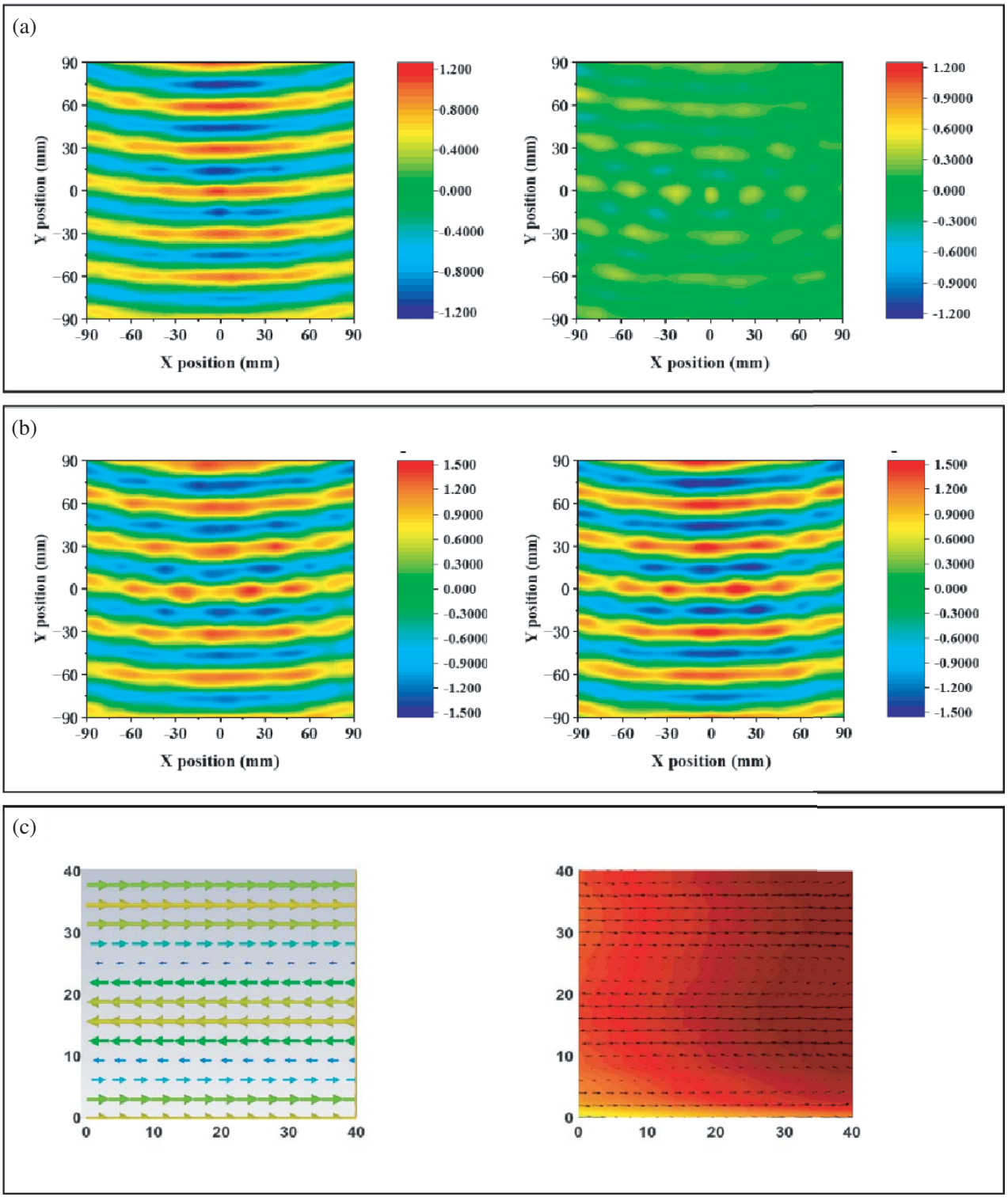

Figure 4. Plane wave measurement results when the antenna is perpendicular or parallel to the magnetic field. (a) Measurement results by a near-field magnetic probe. (b) Measurement results by a bare loop antenna. (c) Simulation (left) and experimental (right) results of plane wave vector magnetic field distribution by a near-field magnetic probe.

and we find that the difference is that there is no shielded layer structure with a gap), the air-field tests of plane waves and cylindrical waves have shown relatively positive results.

It can be vividly seen from the measurement results that both small antennas can detect obvious field distribution. Fig. 4 and Fig. 5 show the results of planar wave and cylindrical wave, respectively. However, to figure out whether it is a plane wave or a cylindrical wave, the measurement results of the bare loop antenna are not significantly different from the case where the ring is perpendicular or parallel to the magnetic field, and the measured directivity is limited. However, the field distribution measured by the small shielded loop antenna is obviously disparate in two directions.

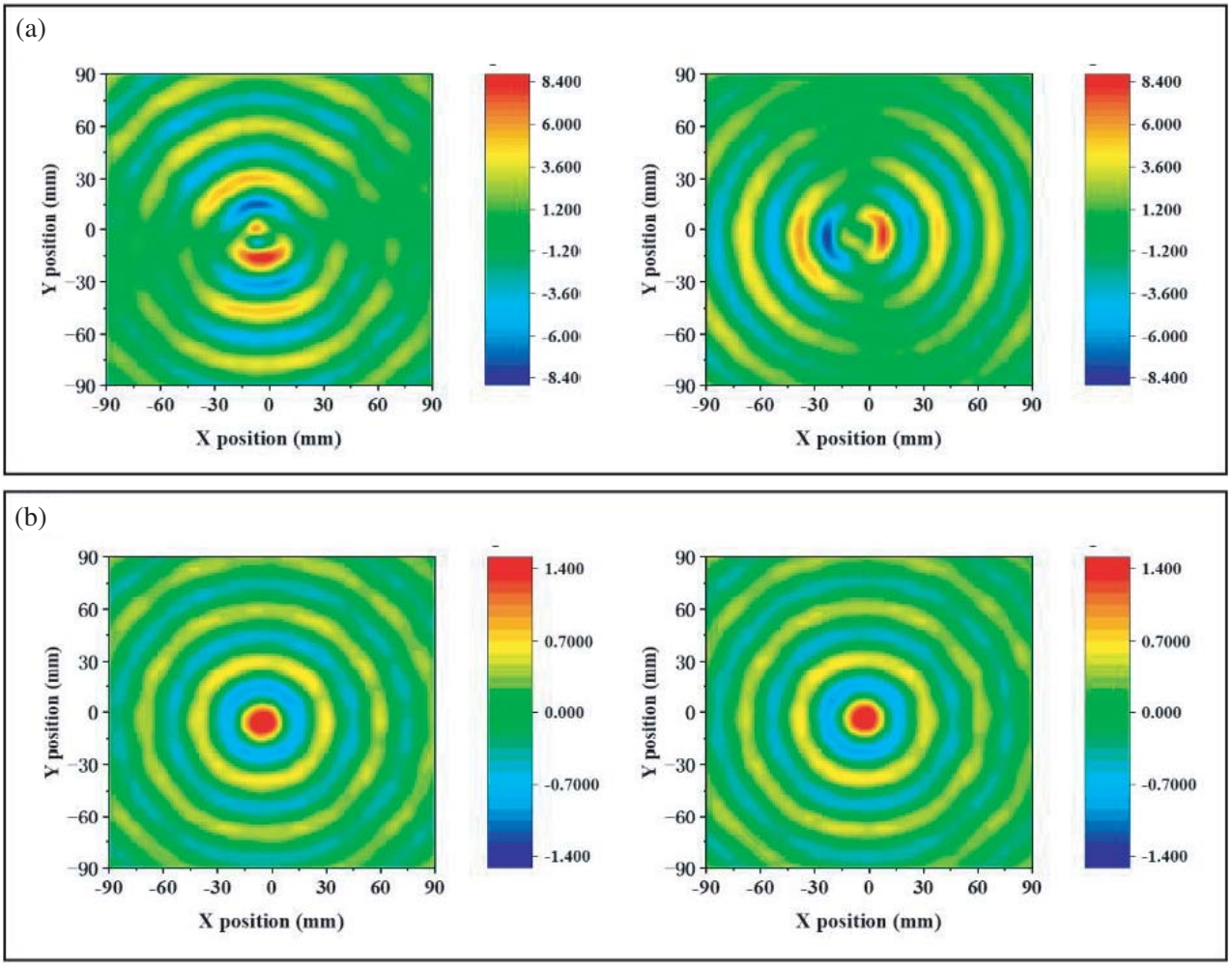

Figure 5. Cylindrical wave measurement results when the ring is perpendicular to the magnetic field and parallel to the magnetic field. (a) Measurement results of the shielded loop antenna. (b) Measurements results of the bare loop antenna.

By synthesizing the magnetic field distribution measurement results of the small loop perpendicular to and parallel to the magnetic field, the vector two-dimensional magnetic field distribution can be obtained. Taking the above measurement result of the plane wave as an example, the vector magnetic field distribution obtained is as shown in Fig. 4(c).

The above experimental results verify the high sensitivity and anisotropic response features of the shielded loop antenna and provide reliability for subsequent measurement of vector magnetic field distribution near metamaterial samples.

3.4. Magnetic Field Distribution Measurement of a Metal Split Ring

Metal split ring resonator is a typical metamaterial unit. The analysis and measurement of the magnetic field distribution of the split ring resonator are of great significance for understanding the working mechanism and lay a solid foundation for the magnetic field distribution measurement of other metamaterial samples.

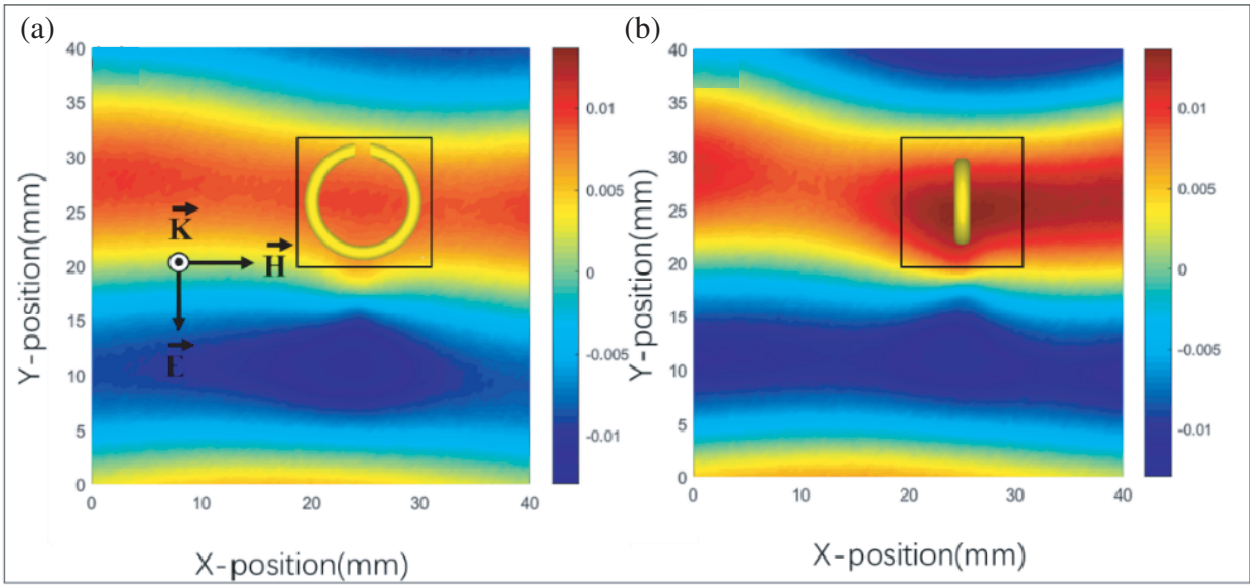

Figure 6. Magnetic field distribution near a split resonant ring with the exciting of Plane wave at the frequency of 8.8 GHz. (a) The ring is parallel to the magnetic field. (b) The ring perpendicular to the magnetic field.

As shown in Fig. 6(b), the small split ring resonance enhances the magnetic field at the resonant frequency when the antenna toroid is perpendicular to the magnetic field, while the magnetic field does not enhance it when the antenna torus is parallel to the magnetic field [Fig. 6(a)]. In other words, metal split ring resonators are capable of adjusting the strength of the magnetic field.

4. CONCLUSIONS

As mentioned above, we have proposed a highly-sensitive near-field magnetic probe and experimentally measured the vector distribution of the near magnetic field, and a processing technology with high efficiency and low cost is proposed. More importantly, the dipole has shown several pros, such as high sensitivity, small sampling interval, and anisotropic measurement. Additionally, according to anisotropic measuring result, the vector magnetic field is derived. Then the antenna can be used to measure vector magnetic field distribution near a metal split ring. The measurement of the distribution of high-frequency vector magnetic fields provides a feasible method for studying the near-field distribution of meta-material samples, which will contribute to its development.

5. FUNDING

Beijing Municipal Science & Technology Commission (No. Z191100004819001); National Natural Science Foundation of China (51872154, 61905021); Science and Technology Plan of Shenzhen City (JCYJ20170817162252290); Basic Research Freedom Exploration Project of Shenzhen (JCYJ20180305164708625); Opening Foundation of State Key Laboratory of Millimeter Waves (K202008); Chinese State Key Laboratory of Tribology.

6. DISCLOSURES

The authors declare no conflicts of interest.

7. ORIGINAL CONTRIBUTION

The near magnetic field of metamaterial sample has an essential impact on revealing its local mechanism of action. However, those experiments in metamaterial field always limit themselves in the measure of the far-field macroscopic and near-field electric measurements, but seldom comes to near magnetic field, considering its difficulty to isolate the disturbance of electric field and overcome processing technology limitations. Therefore, we design and fabricate a magnetic probe, with 1/10 wave length and 20 dB as its rejection ratio, which can combine with parallel double-plate device to become a system that is able to measure vector magnetic field. This heuristic could measure near magnetic field with high frequency directly instead of deducing from electric field. Besides, the most essential creation is that the device could measure the anisotropy of the field's distribution with intervals as small as possible. Moreover, it provides us with a reliable researching method, for instance, for some metamaterial which need to explicit its distribution characteristic of magnetic field, such as Toroidal dipole modes. Partial measure of magnetic field could serve as an efficient tool to reveal the mutual mechanism of action between electromagnetic wave and metamaterial and exploring the relationship between microscopic structural elements and macroscopic electromagnetic properties.

ACKNOWLEDGMENT

The authors gratefully acknowledge discussions with Prof. Zhenghe Feng and Prof. Yue Li.

REFERENCES

1. Pendry, J. B., "Beyond metamaterials," *Nat. Mater*, Vol. 5, No. 10, 763–764, 2006.
2. Smith, D. R., S. Schultz, P. Markos, and C. M. Soukoulis, "Determination of effective permittivity and permeability of metamaterials from reflection and transmission coefficients," *Phys. Rev. B*, Vol. 65, No. 19, 195104, 2001.
3. Justice, B. J., J. J. Mock, L. Guo, A. Degiron, and D. R. Smith, "Spatial mapping of the internal and external electromagnetic fields of negative index metamaterials," *Opt. Express*, Vol. 14, No. 19, 8694–8705, 2006.
4. Bi, K., Y. Guo, J. Zhou, G. Dong, H. Zhao, Q. Zhao, Z. Xiao, X. Liu, and C. Lan, "Negative and near zero refraction metamaterials based on permanent magnetic ferrites," *Sci. Rep.*, Vol. 4, 4139, 2014.
5. Schurig, D., J. J. Mock, B. J. Justice, S. A. Cummer, J. B. Pendry, A. F. Starr, and D. R. Smith, "Metamaterial electromagnetic cloak at microwave frequencies," *Science*, Vol. 314, No. 5801, 977–980, 2006.
6. Liu, R., C. Jic, J. J. Mock, J. Y. Cui, and D. R. Smith, "Broadband ground-plane cloak," *Science*, Vol. 323, No. 5912, 366–369, 2009.
7. Landy, N. and D. R. Smith, "A full-parameter unidirectional metamaterial cloak for microwaves," *Nat. Mater*, Vol. 12, No. 1, 25–28, 2013.
8. Peng, R. G., Z. Q. Xiao, Q. Zhao, F. L. Zhang, Y. G. Meng, B. Li, J. Zhou, Y. C. Fan, P. Zhang, N. H. Shen, T. Koschny, and C. M. Soukoulis, "Temperature-controlled chameleonlike cloak," *Phys. Rev. X*, Vol. 7, 011033, 2017.
9. Cheng, Q., T. J. Cui, W. X. Jiang, and B. G. Cai, "An omnidirectional electromagnetic absorber made of metamaterials," *New J. Phys.*, Vol. 12, No. 6, 063006, 2010.
10. Zhao, Q., Z. Q. Xiao, F. L. Zhang, J. M. Ma, M. Qiao, Y. G. Meng, C. W. Lan, B. Li, J. Zhou, P. Zhang, N. H. Shen, T. Koschny, and C. M. Soukoulis, "Tailorable zero-Phase delay

of subwavelength particles toward miniaturized wave manipulation devices," *Adv. Mater.*, Vol. 27, 6187, 2015.

11. Zhao, Q., L. Kang, B. Du, H. Zhao, Q. Xie, X. Huang, B. Li, J. Zhou, and L. Li, "Experimental demonstration of isotropic negative permeability in a three-dimensional dielectric composite," *Phys. Rev. Lett.*, Vol. 101, 027402, 2008.
12. Yang, X. M., X. Y. Zhou, Q. Cheng, H. F. Ma, and T. J. Cui, "Diffuse reflections by randomly gradient index metamaterials," *Opt. Lett.*, Vol. 35, No. 6, 808–810, 2010.
13. Kaelberer, T., V. A. Fedotov, N. Papasimakis, D. P. Tsai, and N. I. Zheludev, "Toroidal dipolar response in a metamaterial," *Science*, Vol. 330, No. 6010, 1510–1512, 2010.
14. Guo, L. Y., M. H. Li, Q. W. Ye, B. X. Xiao, and H. L. Yang, "Electric toroidal dipole response in split-ring resonator metamaterials," *Phys. Condens. Matter*, Vol. 85, No. 6, 208–471, 2012.
15. Basharin, A. A., M. Kafesaki, E. N. Economou, C. M. Soukoulis, V. A. Fedotov, V. Savinov, and N. I. Zheludev, "Dielectric metamaterials with toroidal dipolar response," *Phys. Rev. X*, Vol. 5, No. 1, 1–11, 2015.
16. Xu, S., A. Sayanskiy, A. S. Kupriianov, V. R. Tuz, P. Kapitanova, H. Sun, W. Han, and Y. S. Kivshar, "Experimental observation of toroidal dipole modes in all-dielectric metasurfaces," *Adv. Opt. Mater.*, Vol. 7, No. 4, 1801166, 2018.
17. Carobbi, C. F. M., L. M. Millanta, and L. Chiosi, "The high-frequency behavior of the shield in the magnetic-field probes," *IEEE Int. Symp. Electromagn. Compat.*, Vol. 1, 35–40, 2000.
18. Balanis, C. A., *Antenna Theory: Analysis and Design*, Harper & Row, 1996.